Solar Energy 139 (2016) 228–237

Contents lists available at ScienceDirect

Solar Energy

journal homepage: www.elsevier.com/locate/solener

Power generation quality analysis and geometric optimization for solar chimney power plants

Jianlan Li [a,*], Hongjing Guo [a,b], Shuhong Huang [a]

[a] Huazhong University of Science and Technology, Wuhan 430074, China
[b] Wuhan Second Ship Design and Research Institute, Wuhan 430200, China

ARTICLE INFO

Article history:
Received 17 September 2015
Received in revised form 9 July 2016
Accepted 26 September 2016

Keywords:
Solar chimney power plant
Streamlined unsteady mechanism model
Power quality factor
Geometric optimization

ABSTRACT

Solar chimney power plant (SCPP) is one of the promising power generation approaches for future applications of solar energy. An unsteady comprehensive mechanism model and a streamlined unsteady mechanism model of SCPPs are derived to analyze the energy conversion and transmission of the system in this paper. The streamlined unsteady mechanism model with concise expressions clearly indicates the correlations among the power output and geometric parameters. Both of the two models are verified by the experimental data from the Spain Manzanares demonstration plant. Moreover, a power quality factor is defined to evaluate the power generation quality of SCPPs both from the points of generation efficiency and power stability. The suitability of the geometric optimization of SCPPs based on the streamlined unsteady mechanism model is finally verified by an example. The coupling optimization results show that there are a strong positive correlation between the chimney height and the power quality factor, as well as a negative correlation between the solar collector radius and the power quality factor. Furthermore, the optimal solar collector height is a quadratic function relation with the chimney diameter, while the optimal thickness of the heat storage layer is little associated with other geometric parameters.

1. Introduction

The solar chimney power plant (SCPP) is a renewable energy device which has advantages of simple technology, low operation cost and continuous generation over other solar power plants (Zhou and Xu, 2016). A typical SCPP is generally composed of a circular solar collector, a chimney at the center of the collector, turbine generators at the bottom of the chimney, and the heat storage layer, as shown in Fig. 1.

During the day, solar radiation penetrates the transparent collector to warm the heat storage layer. Some heat energy is stored in the heat storage layer, while the other heat energy is transferred to the airflow on the heat storage layer surface by convection. The warm airflow accelerates along the solar collector to the bottom of the chimney, drives the turbine generators to generate electricity, and finally leaves the system from the top of the chimney. At the same time, the ambient air continuously enters the system from the edge of the solar collector, thereby forms the continuous air current. At night or on cloudy days, the heat energy is released from the heat storage layer, which makes the system continuously produce electricity.

The power generation principle and manufacturing technology of SCPPs were proposed by Schlaich (Pasumarthi and Sherif, 1998a, 1998b). The first SCPP prototype plant was built in Manzanares, Spain, and operated between 1982 and 1989 with approximately 50 kW of electrical power output, which demonstrated the technology feasibility of SCPPs (Haaf et al., 1983; Haaf, 1984; Schlaich, 1995). However, due to the huge investement, large occupied area, and poor efficiency, SCPPs has not yet been commercialized until now (Zhou and Xu, 2016).

In recent years, numerous researches have been conducted to study the performance of SCPPs. It was found that the turbine pressure drop ratio, the air velocity at chimney inlet, the chimney friction, as well as meteorological conditions, including solar irradiation, the sunlight zenith angle, the ambient temperature, the temperature lapse rate, the nocturnal temperature inversion, the ambient crosswind and so on, affect the power output of the plant (Gannon and von Backström, 2000; Bernardes et al., 2003; Pretorius and Kröger, 2006a, 2006b, 2009; Nizetic and Klarin, 2010; Ming et al., 2012; Guo et al., 2013, 2015; Hamdan, 2013; Dehghani and Mohammadi, 2014).

* Corresponding author.
E-mail address: hust_ljl@hust.edu.cn (J. Li).

http://dx.doi.org/10.1016/j.solener.2016.09.033
0038-092X/

Nomenclature

Abbreviation

A	area (m^2)
c	specific heat capacity ($J\ kg^{-1}\ K^{-1}$)
D	diameter (m)
f	friction factor
F	power generation fluctuation
Fo	Fourier coefficients
G	solar radiation intensity ($W\ m^{-2}$)
h	heat transfer coefficient ($W\ m^{-1}\ K^{-1}$)
H	height (m)
k	turbine pressure ratio
m	mass flow rate ($kg\ s^{-1}$)
P	power output (kW)
Pr	Prandtl number
p	Pressure (Pa)
q	heat transfer intensity ($W\ m^{-2}$)
QF	power quality factor
R	radius (m)
T	temperature (K)
v	velocity ($m\ s^{-1}$)

Acronym

SCPP	solar chimney power plant
SUMM	streamlined unsteady mechanism model
UCMM	unsteady comprehensive mechanism model

Greek symbols

α	absorption rate
δ	thickness (m)
ε	emissivity
η	efficiency
λ	thermal conductivity ($W\ m^{-1}\ K^{-1}$)
ρ	density ($kg\ m^{-3}$)
γ	reflectivity
σ	Boltzmann constant
τ	transmissivity
v	kinematic viscosity ($N\ s\ m^{-2}$)
Δ	difference

Subscript

a	air
am	ambient air
ch	chimney
col	solar collector
dew	dew point
f	friction
in	inlet
out	outlet
s	heat storage layer
sf	suction force
t	time
te	turbine electricity generation performance
tm	turbine machinery performance

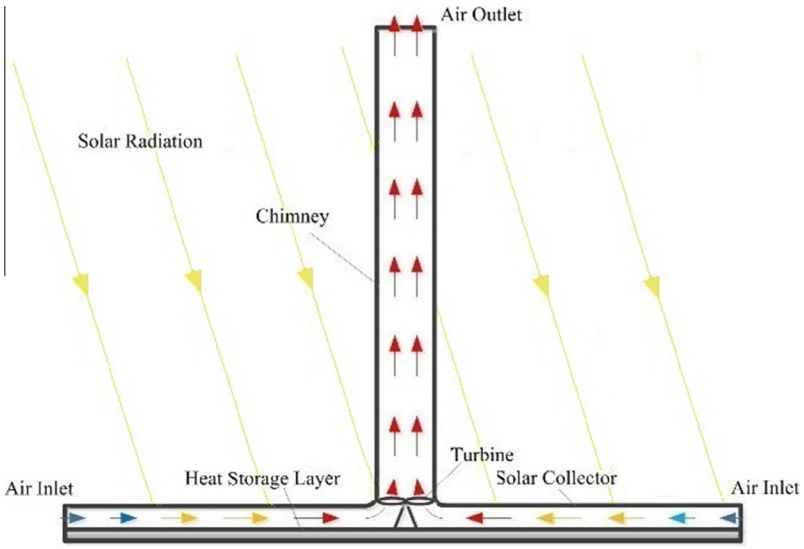

Fig. 1. Schematic overview of a typical solar chimney power plant.

Moreover, it has been verified that geometric parameters significantly impact the performance of SCPPs. Generally, the power output and efficiency increase with its dimension and the energy production cost reduces (Mullett, 1987; Schlaich et al., 2005). And the height and diameter of the chimney, the collector radius are the essential variables for solar chimney design (Zhou et al., 2007, 2009; Maia et al., 2009; Hamdan, 2013). Koonsrisuk et al. (2010) evaluated the ratio of height to radius for the maximum mass flow rate of the plant. In the meanwhile, collector roof shape also impacts the power output of SCPPs and the proper collector roof shape can maximize the power output (Pretorius and Kröger, 2007; Bernardes, 2010; Cottam et al., 2016). Patel et al. (2014) found that the collector inlet opening, the collector outlet height, the collector outlet diameter, the chimney inlet diameter, and the divergence angle of the chimney, significantly influence the overall performance of SCPPs. It was shown that plant power production is a function of the collector roof shape and inlet height (Pretorius and Kröger, 2006b). The SCPP with proper sloping

collector and divergent-top chimney can even boost power output by up to 400% (Koonsrisuk and Chitsomboon, 2013). Besides, Kasaeian et al. (2014) stated that the geometrical parameters have an optimal range including minimum and maximum amounts.

Schlaich (1995) indicated that optimal geometrical dimensions for SCPPs do not exist. But if construction costs are taken into account, optimal plant configurations may be established. Dehghani and Mohammadi (2014) simultaneously took the power output and capital cost as the objective functions to optimize the configuration (collector diameter, chimney height and chimney diameter) of SCPPs. Gholamalizadeh and Kim (2014) developed a triple-objective method for SCPPs to simultaneously optimize the expenditure, the total efficiency and the power generation. Moreover, several other cost models were also presented to evaluate and optimize the configurations of SCPPs (Schlaich et al., 2005; Pretorius and Kröger, 2008; Asnaghi and Ladjevardi, 2012; Alawin et al., 2013; Li et al., 2014; Zou et al., 2013).

Due to the volatility and discontinuity of solar energy, the power stability is one of the critical influences on the grid-connection of solar energy. The heat storage capacity is found to be key for the stability of power output. A larger thermal conductivity of heat storage material results in a better heat storage capacity, therefore decrease the fluctuation of power output (Pretorius and Kröger, 2007). A hybrid energy storage system with water and soil was used to smooth the power output by Ming et al. (2013). Besides, closed water-filled bags/water-filled black tubes, and solid oxide fuel cell, were employed as energy storage materials to make the profile of power output be more uniform (Schlaich et al., 2005; Bernardes and Zhou, 2013; Shariatzadeh et al., 2015). Xu et al. (2015) indicated that the vapor condensation of the moistened air occurring in high chimney can also smooth the daily output profile. Moreover, Papageorgiou (2013) proposed an enclosed solar collector encircled by a peripheral wall, where the power output can be adjusted by controlling the number of opening and thus smooth the power output.

Geometric optimization is important for promoting SCPPs. However, aforementioned publications on geomatric optimization of SCPPs are mostly based on the thermodynamic performance, ignoring the influence of power stability. In fact, the grid does not welcome the power output with low stability, thus the low stability become one of obstacles for the commercial application of SCPPs. Therefore, it is necessary to simultaneously take thermodynamic performance and stability performance into account during the design of SCPPs. In this study, a power quality factor is defined to comprehensively evaluate the power generation quality from two aspects: generation efficiency and power stability of the power output, which tries to assess the power generation acceptability of the grid simultaneously from the view of quantity and quality. Moreover, the geometric optimization of SCPPs in this paper reveals the correlations among the geometric parameters and the power generation quality based on the criterion of the power quality factor.

2. Unsteady mechanism model of solar chimney power plants

2.1. Energy balance of the solar collector

The air flow and energy transfer in the solar collector are numerically simulated by solving equations of a one-dimensional compressible flow. It is assumed that the solar collector and the heat storage layer have same radii. An infinitesimal annulus with radius r is taken for study, as shown in Fig. 2.

The heat absorbed by the solar collector includes the direct solar radiation with the intensity of $\alpha_{col}G^t$ and the reflected radiation from the heat storage layer with the intensity of $\alpha_{col}\gamma_s\tau_{col}G^t$, where superscript t means the real-time parameter for the time t. The radiation intensity between the solar collector and the sky, and between the heat storage layer and the solar collector, are $q^t_{col,sky}$ and $q^t_{s,col}$, respectively. Meanwhile, the convective heat transfer intensity between the solar collector and the indoor air of the solar collector, and between the solar collector and the ambient air, are $q^t_{col,a}$ and $q^t_{col,am}$, respectively.

Then the energy balance of solar collector is as below,

$$\alpha_{col}G^t + \alpha_{col}\gamma_s\tau_{col}G^t + q^t_{s,col} = q^t_{col,sky} + q^t_{col,a} + q^t_{col,am} + c_{col}\rho_{col}\delta_{col}\frac{T^t_{col} - T^{t-1}_{col}}{\Delta t} \quad (1)$$

Since the heat storage layer and the solar collector usually have large areas, both of them can be regarded as large parallel boards. Therefore, the radiation heat transfer intensity between them is,

$$q^t_{s,col} = \frac{1}{\frac{1}{\varepsilon_s} + \frac{1}{\varepsilon_{col}} - 1}\sigma\left[(T^t_s)^4 - (T^t_{col})^4\right] \quad (2)$$

The radiation heat transfer intensity between the solar collector and the sky is,

$$q^t_{col,sky} = \varepsilon_{col}\sigma\left[(T^t_{col})^4 - \left(T^t_{sky}\right)^4\right] \quad (3)$$

where the sky temperature can be calculated according to Liu (2010),

$$T^t_{sky} = T^t_{am}(0.734 + 0.0061T_{dew})^{1/2} \quad (4)$$

The convection heat transfer intensities between the solar collector and the ambient air, and between the solar collector and the indoor air, are calculated as,

$$\begin{cases} q^t_{col,am} = h^t_{col,am}(T^t_{col} - T^t_{am}) \\ q^t_{col,a} = h^t_{col,a}(T^t_{col} - T^t_a) \end{cases} \quad (5)$$

The heat transfer coefficients were defined in detail by Kreetz (1997),

$$\begin{cases} h^t_{col,am} = 3.87 + 0.22\,v^t_{am}\rho^t_{am}c_a/Pr_a^{2/3} \\ h^t_{col,a} = 3.87 + 0.22\,v^t_a\rho^t_a c_a/Pr_a^{2/3} \end{cases} \quad (6)$$

2.2. Energy balance of the heat storage layer

The heat storage layer absorbs solar radiation transmitted from the solar collector with the intensity of $\alpha_s\tau_{col}G^t$ and conducts downwards heat with the intensity of q^t_s. Moreover, there are also the radiation heat transfer intensity between the heat storage layer and the solar collector $q^t_{s,col}$, as well as the convective heat transfer intensity between the heat storage layer and the indoor air $q^t_{s,a}$.

The energy balance at the surface of the heat storage layer is,

$$\alpha_s\tau_{col}G^t = q^t_{s,col} + q^t_{s,a} + q^t_s \quad (7)$$

where the heat storage intensity q^t_s is associated with the solar radiation intensity, the radiation heat transfer intensity between the heat storage layer and the solar collector, and the convective heat transfer intensity between the heat storage layer and the indoor air. The convective heat transfer intensity between the heat storage layer and the indoor air of the solar collector is,

$$q^t_{s,a} = h^t_a(T^t_s - T^t_a) \quad (8)$$

In order to improve the storage performance, insulation materials are often laid at the bottom and around the surface of the heat storage layer to reduce energy loss. Since the heat conduction in the radial direction is much weaker than that in the vertical direction, the heat storage layer of SCPPs can be approximately regarded as a one-dimensional unsteady heat transfer model with

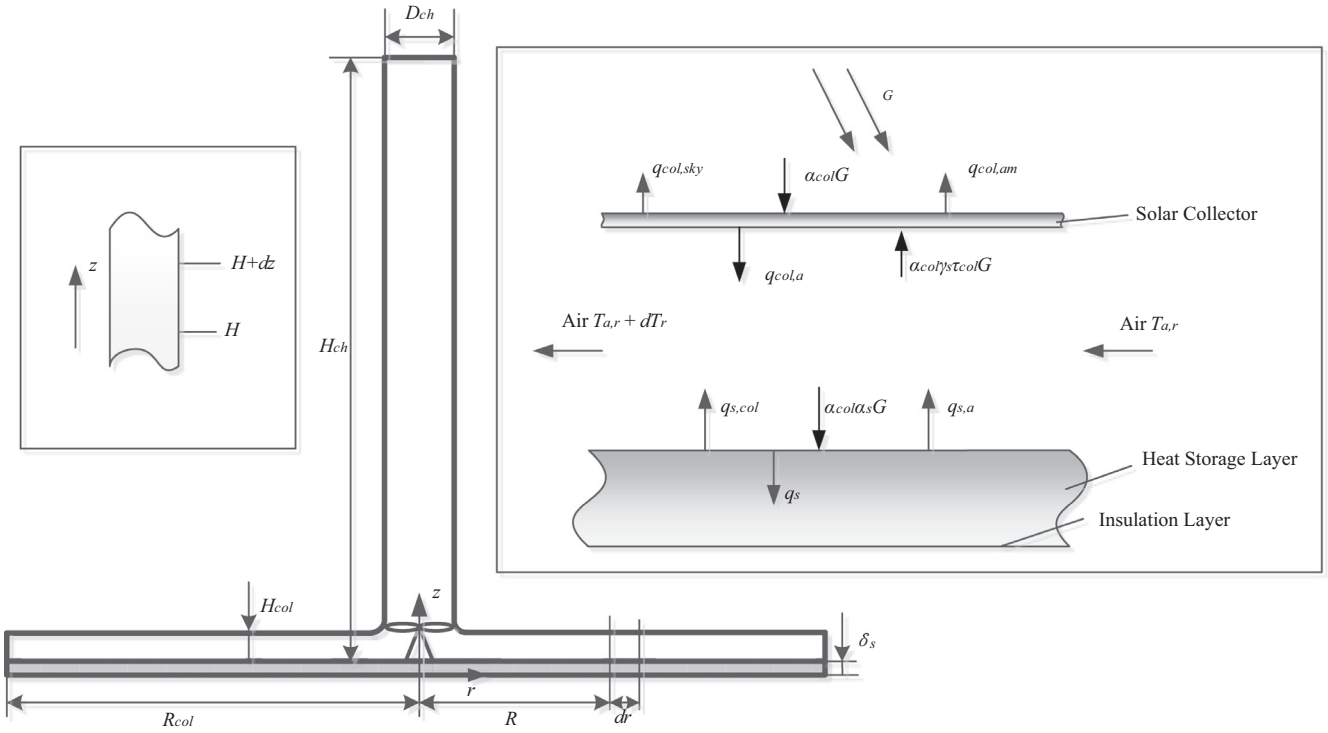

Fig. 2. Heat transfer analysis of solar chimney power plants.

a limited thickness δ_s and an adiabatic surface. The heat transfer of the heat storage layer can be described as the one-dimensional Fourier-Biot diffusion equation (Pretorius and Kröger, 2006b),

$$\lambda_s \frac{\partial^2 T_{s,z}}{\partial z^2} = c_s \rho_s \frac{\partial T_{s,z}}{\partial \tau} \tag{9}$$

The initial conditions and boundary conditions are as below,

$$\begin{cases} \tau = 0 \; 0 < z < \delta_s & T_{s,z} = T_{am} \\ \tau > 0 \; z = 0 & T_{s,z} = T_s \\ \tau > 0 \; z = \delta_s & \frac{\partial T_{s,z}}{\partial z} = -\frac{q_s}{\lambda_s} \end{cases} \tag{10}$$

The solution of Eq. (9) is derived as (Tu et al., 1992),

$$\begin{cases} T_s^t = T_s^0 + \sum_{n=1}^{t} q_s^n \frac{\Delta t}{\rho_s c_s \delta_s} + \frac{\delta_s q_s^t}{3\lambda_s} + \frac{\delta_s}{\lambda_s} \sum_{n=1}^{\infty} B_n^t \left[-\frac{\cos(n\pi)}{n\pi} \right] \exp[-(n\pi)^2 F_o] \\ B_n^t = \frac{2(-1)^n}{n\pi} q_s^t + \sum_{i=1}^{t-1} B_n^i \{\exp[-(n\pi)^2 F_o] - 1\} \\ B_n^1 = \frac{2(-1)^n}{n\pi} q_s^1 \end{cases} \tag{11}$$

It can be seen from Eq. (11) that the surface temperature of the heat storage layer T_s^t depends on the initial temperature of the heat storage layer T_s^0, the accumulative thermal energy storage $\sum_{n=1}^{t} q_s^n \frac{\Delta t}{\rho_s c_s \delta_s}$, the temperature distribution of the heat storage layer $\frac{\delta_s q_s^t}{3\lambda_s}$, and the instantaneous thermal conduction $\frac{\delta_s}{\lambda_s} \sum_{n=1}^{\infty} B_n^t \left[-\frac{\cos(n\pi)}{n\pi} \right] \exp[-(n\pi)^2 F_o]$.

In order to easily observe the factors which affect the surface temperature of the heat storage layer, Eq. (11) is translated into,

$$\begin{cases} T_s^t = T_s^0 + K_1^t + K_2 q_s^t \\ K_1^t = \frac{\Delta t}{\rho_s c_s \delta_s} \sum_{i=1}^{t-1} q_s^n + \frac{\delta_s}{\lambda_s} \sum_{n=1}^{\infty} \sum_{i=1}^{t-1} B_n^i \left[-\frac{\cos(n\pi)}{n\pi} \right] \{\exp[-2(n\pi)^2 Fo] \\ \qquad - \exp[-(n\pi)^2 F_o]\} \\ K_2 = \frac{\Delta t}{\rho_s c_s \delta_s} + \frac{\delta_s}{3\lambda_s} + \frac{\delta_s}{\lambda_s} \sum_{n=1}^{\infty} \frac{2(-1)^n}{n\pi} \left[-\frac{\cos(n\pi)}{n\pi} \right] \exp[-(n\pi)^2 F_o] \end{cases} \tag{12}$$

where T_s^t is expressed as the sum of T_s^0, K_1 and $K_2^t q_s^t$. T_s^0 indicates the constant influence of the initial condition on the temperature for any time. K_1^t is related to physical parameters of the heat storage layer (including the heat capacity, the thermal conductivity, the density, the thickness of the heat storage layer and so on) and the accumulative thermal energy storage before time t. K_2 is the function of physical parameters and $K_2 q_s^t$ denotes the thermal energy storage capacity at time t.

2.3. Energy balance of the air

The convective heat transfers between the indoor air and the heat storage layer, as well as between the indoor air and the solar collector, increase the air temperature and reduce its density. Due to the pressure created by the density difference between the indoor air and the ambient air, the air is driven to flow in the solar collector toward the chimney. The energy balance of the indoor air is,

$$\int_{D_{ch}/2}^{R_{col}} 2\pi r \left[h_a^t (T_{col}^t - T_a^t) + h_a^t (T_s^t - T_a^t) \right] dr = \int_{T_{am}^t}^{T_{a,ch}^t} m_a^t c_a dT_{a,r}^t \tag{13}$$

It can be seen from Eq. (13) that the air temperature is affected by the surface temperatures of the heat storage layer the solar collector, the heat transfer coefficient, and the air mass flow rate. It is obviously that the air temperature has positive correlations with the temperature difference between the air and the solar collector as well as between the air and the heat storage layer, along with the heat transfer coefficient.

2.4. Pressure loss

The density difference between the air at the bottom of the chimney and the ambient air creates a suction force which acts as the driving force of the air flow. Besides, the pressure difference between the inlet air of the chimney $\rho_{a,ch}^t$ and the ambient air ρ_{am}^t is less than 4 Pa (Ming et al., 2006), thus the ratio of density $\rho_{a,ch}^t / \rho_{am}^t$ can be substituted of the ratio of temperature $T_{am}^t / T_{a,ch}^t$.

Therefore, the suction force is expressed in Eq. (14) according to Bernoulli's principle,

$$p_{sf}^t = \int_{\delta_s}^{H_{ch}+\delta_s} \left(\rho_{a,ch}^t - \rho_{am}^t\right) g dz = \rho_{am}^t \left(1 - \frac{T_{am}^t}{T_{a,ch}^t}\right) g H_{ch} \tag{14}$$

Since there are frictions between the air and the collector, and between the air and the chimney wall, the pressure loss in the system can be calculated as below (Haaf et al., 1983).

$$p_f^t = \frac{f_{col} R_{col}}{2\rho_{am}^t H_{col}} \left(\frac{m_a^t}{2\pi R_{col} H_{col}}\right)^2 + \frac{2 f_{ch} H_{ch}}{\rho_{a,ch}^t D_{ch}} \left(\frac{m_a^t}{\pi D_{ch}^2/4}\right)^2 \tag{15}$$

In order to ensure the continuous air flow, the suction force must overcome the all frictions in the collector and in the chimney,

$$p_{sf}^t = p_f^t \tag{16}$$

Thus, according to Eqs. (14)–(16),

$$\rho_{am}^t \left(1 - \frac{T_{am}^t}{T_{a,ch}^t}\right) g H_{dt} = \left(\frac{f_{col}}{8\pi^2 \rho_{am}^t R_{col} H_{col}^3} + \frac{32 f_{ch} H_{ch}}{\pi^2 \rho_{a,ch}^t D_{ch}^5}\right) \left(m_a^t\right)^2 \tag{17}$$

2.5. Turbine generator unit

Turbine generator unit is placed at the bottom of the chimney to transfer the kinetic energy of the air flow into the electricity power. The power output of the unit is,

$$P^t = \eta_{te} \eta_{tm} \frac{m_a^t}{\rho_{a,ch}^t} p_{tur}^t \tag{18}$$

where the pressure drop of the turbine is,

$$\Delta p_{tur}^t = k p_{sf}^t \tag{19}$$

Therefore, Eqs. (1)–(19) constitute the unsteady comprehensive mechanism model (UCMM) of SCPPs with thermal storage layer. It can be seen from Eq. (18) that, the power output of SCPPs is proportional to the mass flow rate and the temperature rise of the indoor air.

2.6. The streamlined mechanism model of solar chimney power plants

The UCMM embodies the energy conversion and transmission in SCPPs. However, the expression of the UCMM is too complex and it is difficult to distinguish the influence of the system structure on the power output of SCPPs. Thus, a streamlined model of SCPPs is derived based on following assumptions.

A. The radiation heat transfers between the solar collector and the sky, as well as between the solar collector and the heat storage layer, can be ignored in Eqs. (1) and (7). It is because the temperatures of the solar collector, the heat storage layer and the sky are relatively not high as well as temperature differences among them are relatively low.
B. The convective heat transfer coefficients between the ambient air and the solar collector, and between the indoor air and the solar collector, as well as between the indoor air and the heat storage layer, change little in the system, which has a very small impact on the power output of SCPPs, thus these coefficients can be regarded as constants.
C. Due to the small temperature differences among the air in the chimney, the indoor air, and the ambient air, the air temperature difference ratio $\left(1 - \frac{T_{am}^t}{T_{a,ch}^t}\right)$ in Eq. (17) can be replaced by $\frac{T_a^t - T_{am}^t}{T_{am}^t}$.

Based on above assumptions, Eqs. (1), (7), (12) and (13) are simplified into Eq.(20), and Eq. (17) is simplified into Eq. (21).

$$\left(\frac{\alpha_{col} + \tau_{col}\gamma_s}{h_a + h_{col,am}} + \frac{K_1 \alpha_s \tau_{col}}{K_1 h_a + 1}\right) G^t + \frac{K_2^t}{K_1 h_a + 1} = \left[\frac{8\pi R_{col} H_{col} Pr^{2/3} c_a (h_a - 3.87)}{0.11 \rho_{am}^t c_a \left(4R_{col}^2 - D_{ch}^2\right) h_a} + \frac{h_{col,am}}{h_a + h_{col,am}}\right] \left(T_a^t - T_{am}^t\right) \tag{20}$$

$$\frac{T_a^t - T_{am}^t}{T_{am}^t} g H_{ch} = \left(\frac{f_{col}}{16\pi^2 \rho_{am}^t R_{col} H_{col}^3} + \frac{16 f_{ch} H_{ch}}{\pi^2 \rho_{a,ch}^t D_{ch}^5}\right) \left(m_a^t\right)^2 \tag{21}$$

It can be derived from Eq. (20) and Eq. (21) that,

$$\begin{cases} T_a^t - T_{am}^t = \frac{C_1^t}{\frac{C_2^t R_{col} H_{col}}{4R_{col}^2 - D_{ch}^2} + C_3^t} \\ C_1^t = \left(\frac{\alpha_{col} + \tau_{col}\gamma_s}{h_a + h_{col,am}} + \frac{K_1 \alpha_s \tau_{col}}{K_1 h_a + 1}\right) G^t + \frac{K_2^t}{K_1 h_a + 1} \\ C_2^t = \frac{8\pi Pr^{\frac{2}{3}} (h_a - 3.87)}{0.11 \rho_{am}^t h_a} \\ C_3^t = \frac{h_{col,am}}{h_a + h_{col,am}} + \frac{1}{K_1 h_a + 1} \end{cases} \tag{22}$$

$$\begin{cases} \left(m_a^t\right)^2 = \frac{C_4^t H_{ch} \left(T_a^t - T_{am}^t\right)}{\frac{C_5^t}{R_{col} H_{col}^3} + \frac{C_6^t H_{ch}}{D_{ch}^5}} \\ C_4^t = \frac{g}{T_{am}^t} \\ C_5^t = \frac{f_{col}}{16\pi^2 \rho_{am}^t} \\ C_6^t = \frac{16 f_{ch} H_{ch}}{\pi^2 \rho_{a,ch}^t} \end{cases} \tag{23}$$

It can be seen from Eq. (22) that the air temperature difference between the ambient air and the indoor air is related with system geometric parameters, including the solar collector height H_{col}, the solar collector radius R_{col} and the chimney diameter D_{ch}. The air temperature difference increases with the increase of the solar collector radius and the decrease of the solar collector height and the chimney radius. The coefficient C_1^t reflects the impact of the solar radiation and the thermal energy storage on the air temperature rise. C_2^t and C_3^t reflect the influence of convective heat transfer coefficient on the air temperature rise. The thermal energy stored in the heat storage layer increases with the increase of solar radiation, which results in the increases of the coefficient C_1^t and the air temperature rise. If the convection heat transfers between the air and the solar collector and between the air and the heat storage, increase, then the coefficient C_2^t increases while C_3^t decreases. With the increase of the convection heat transfer coefficient $h_{col,am}$ between the solar collector and the ambient air, C_3^t increases and the air temperature rise decreases.

In Eq. (23), the air mass flow m_a^t depends on the air temperature rise, the chimney height H_{ch}, the chimney diameter D_{ch}, the solar collector radius R_{col}, and the solar collector height H_{col}. When the solar collector height H_{col} is small, m_a^t is dramatically influenced by H_{col} and increases with the increase of H_{col}. However, when H_{col} increases to a certain value, $\frac{C_5^t}{R_{col} H_{col}^3}$ becomes very small and $\frac{C_5^t}{R_{col}} \ll \frac{C_5^t}{H_{col}^3} \ll C_6^t H_{ch}$. Then the air mass flow will mainly positively correlate with the chimney diameter.

Put Eqs. (21) and (22) into Eq. (18), the streamlined unsteady mechanism model (SUMM) of SCPP can be obtained as,

$$P^t = \frac{k \eta_{te} \eta_{tm} \left[C_1^t C_4^t H_{ch} \Big/ \left(\frac{C_2^t R_{col} H_{col}}{4R_{col}^2 - D_{ch}^2} + C_3^t\right)\right]^{1.5}}{\left(\frac{C_5^t}{R_{col} H_{col}^3} + \frac{C_6^t H_{ch}}{D_{ch}^5}\right)^{0.5}} \tag{24}$$

Obviously, Eq. (24) provides a concise expression of the power output of SCPPs which is much simpler than that of the UCMM. It can be seen from Eq. (24) that the power output is closely related to system geometric parameters. The power output has obvious positive correlations with the solar collector radius R_{col} and the chimney height H_{ch}. Since the increase of the chimney diameter decreases the air temperature rise and increases the air mass flow, while the power output is proportion to the air temperature rise and the air mass flow, therefore, the chimney diameter has double influence on the output power. Thus, there exists an optimum chimney diameter to make the maximum power output of SCPPs. Due to the concise expression of the SUMM, it provides a reliable and fast way to optimize the geometric parameters of SCPPs.

3. Power generation quality evaluation of solar chimney power plants

The generation efficiency is an important indicator to reflect the availability of energy in thermal power plants. However, due to the instability and discontinuity of solar energy, the power output of solar plants is obviously unstable. Thus, when solar plants connect to the grid, it inevitably results in the increase of the power regulation load and threats the safe operation of the grid seriously. Especially, the grid will face a high risk of scheduling when solar plants connect to the grid in large-scale. So, not only the generation efficiency but also the power stability shall be considered in the design of SCPPs. With the improvement of the power stability, the disturbance of SCPPs on the grid reduces and then SCPPs can be more easily accepted by the grid.

The generation efficiency of SCPPs is defined as the ratio of the system electricity output and the solar radiation within 24 h,

$$\eta_{SCPP} = \frac{\sum P^t}{A_{col}\sum G^t} = \frac{\sum P^t}{\left(\pi R_{col}^2\right)\sum G^t} \tag{25}$$

The power fluctuation of SCPPs is defined as the ratio of the power output variation and the power output for the time t, which reflects the transient impact of the power change on the grid. Then, the power fluctuation per day is defined as the average power fluctuation rate within 24 h,

$$F_{SCPP} = \frac{\sum |P^{t+1} - P^t|}{nP^t} \tag{26}$$

Thus, (1 − F) is the power stability of SCPPs. The smaller the fluctuation is, the better the system stability will be. In order to take into account the influence of the generation efficiency and the power stability of SCPPs on the grid, a new generation performance evaluation index, power quality factor, is defined as,

$$QF_{SCPP} = (1 - F_{SCPP})\eta_{SCPP} = \left(1 - \frac{\sum |P^{t+1} - P^t|}{nP^t}\right)\frac{\sum P^t}{\left(\pi R_{col}^2\right)\sum G^t} \tag{27}$$

Obviously, the higher power quality factor means the better generation efficiency and the better power stability, which indicates the higher acceptability of SCPPs by the grid. It can be seen from Eqs. (24) and (27) that the generation performance of SCPPs is closely related to the system geometric parameters, including the height and the diameter of the chimney, the radius and the height of the solar collector, and the thickness of the heat storage layer.

4. Results and discussion

4.1. Model validation

According to the UCMM and the SUMM of SCPPs presented in this paper, the power output of the Spain Manzanares demonstration power plant is simulated by engineering equation solver (EES). The flow chart of the simulation process in EES is shown in Fig. 3. In this case, the daily solar radiation comes from Schlaich et al. (2005). The solar collector is made of glass and the heat storage layer is made of soil. The plant-related parameters are shown in Table 1 and optical properties are as below,

$$\begin{cases} \alpha_{col} = \varepsilon_{col} & \gamma_{col} = 0 & \tau_{col} = 1 - \varepsilon_{col} \\ \alpha_s = \varepsilon_s & \gamma_s = 1 - \varepsilon_s & \tau_s = 0 \end{cases}$$

The simulation results are compared with the measured data (1987/06/08) (Schlaich et al., 2005) in Table 2 and Fig. 4. It is indicated that both of the UCMM and the SUMM have satisfactory consistency with the experiment data. It can be seen that three curves of the power output have similar trends in Fig. 4. As shown in Table 2, the errors of the power output between the UCMM and the experimental data, as well as between the SUMM and experimental data, are 3.57% and 3.24%, respectively. Besides, the comparisons of VRMSE and NMBE between two models and experimental data are less than 15%. Especially, the error differences between the UCMM and the SUMM are relatively small. The results show that the assumptions in Section 2.6 are reasonable and the SUMM is reliable.

4.2. Performance analysis of SCPPs

Based on the SUMM, the control variable method is employed to discuss the correlations among the generation efficiency, the power stability, the power quality, and the geometric parameters. The analysis results are shown in Figs. 5–7. The original values of geometric parameters are shown in Table 3 and other parameters are the same as those in Table 1.

4.2.1. The influences of geometric parameters on the generation efficiency

The influences of geometric parameters on the generation efficiency are shown in Fig. 5. It is obvious that the generation efficiency is mainly affected by the chimney height H_{ch}. Fig. 5 shows a strong positive correlation between H_{ch} and the generation efficiency. Eqs. (14) and (19) indicate that the power output is

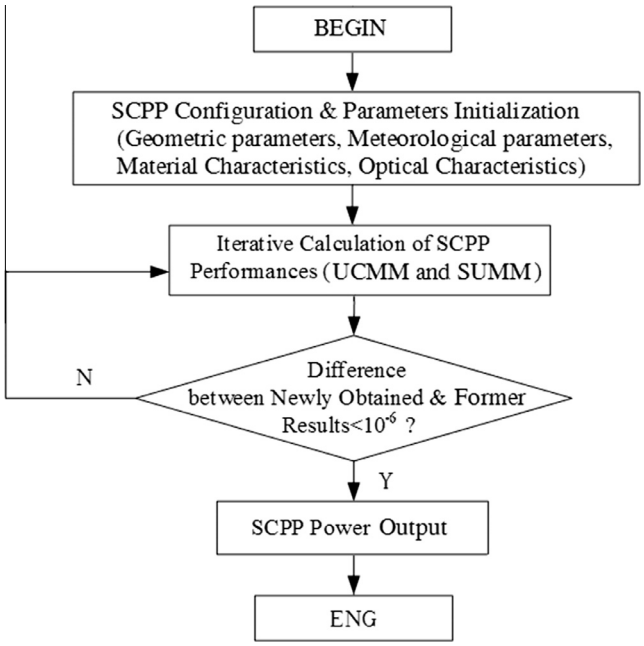

Fig. 3. Flow chart of the simulation process in the EES.

Table 1
Parameters of the Spain Manzanares demonstration power plant (Haaf et al., 1983).

Item	Value
Collector radius (m)	122
Collector height (m)	1.85
Chimney diameter (m)	10.16
Chimney height (m)	194.6
Glass emissivity	0.21
Soil emissivity	0.9
Turbine pressure drop coefficient	2/3
Turbine-machinery efficiency	0.75
Turbine generation efficiency	0.85
Soil density (kg m^{-3})	1793.6
Soil heat capacity (J kg^{-1} K^{-1})	911
Soil thermal conductivity (W m^{-1} K^{-1})	1.1
Heat storage layer thickness (m)	5.7
Ambient temperature (K)	297.57 ± 3.83
Dew point temperature (K)	275.01
External wind speed (m s^{-1})	5

Table 2
Error analysis of the UCMM and the SUMM.

	Experimental data	UCMM	SUMM
Power output (kW h)	363.9	376.9	375.8
Relative error of power output (%)	–	3.6	3.2
Coefficient of variation of the root mean square error (VRMSE) (%)	–	12.4	13.3
Normalized mean bias error (NMBE) (%)	–	9.8	10.5

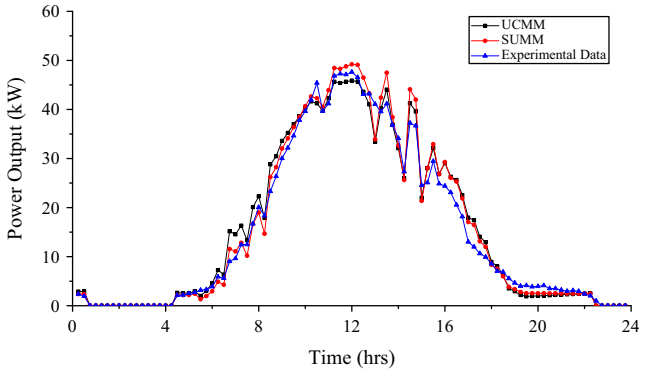

Fig. 4. Power output comparisons of the UCMM and the SUMM with experiment data.

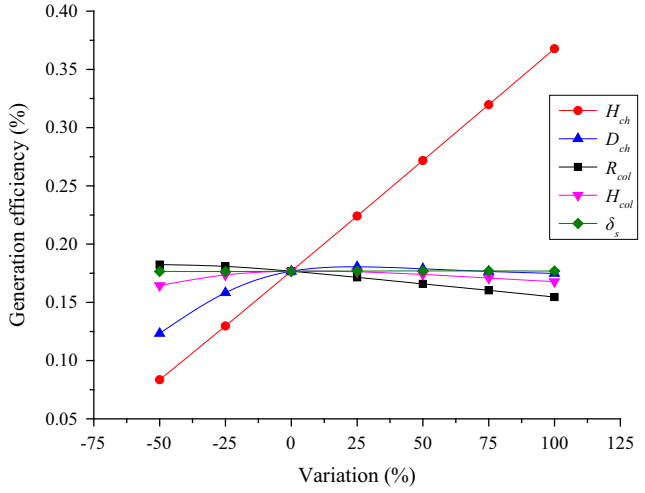

Fig. 5. Influences of geometric parameters on generation efficiency.

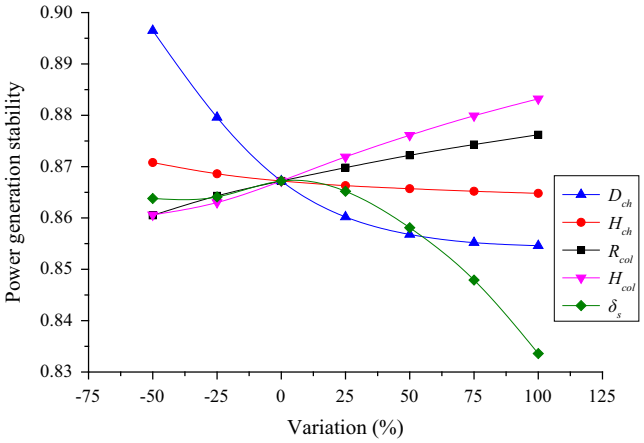

Fig. 6. Influences of geometric parameters on power stability.

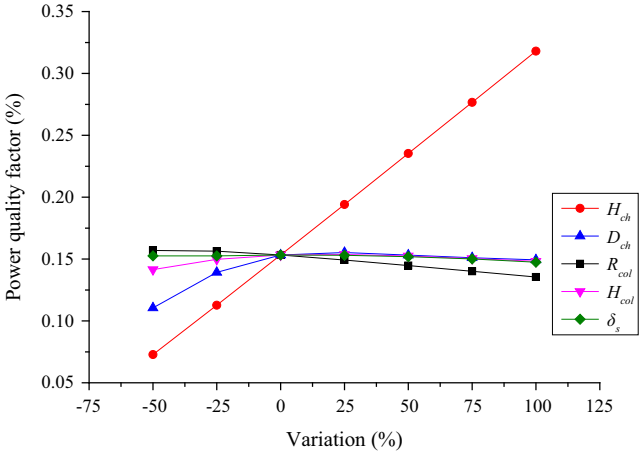

Fig. 7. Influences of geometric parameters on power quality factor.

Table 3
Original values of geometric parameters.

Geometric parameter	Original value
Collector radius (m)	270
Collector height (m)	1.5
Chimney diameter (m)	30
Chimney height (m)	200
Heat storage layer thickness (m)	2.0

proportional to the suction force and the suction force increases with the increase of the chimney height. So, the generation efficiency increases linearly from 0.08% to 0.37% when H_{ch} increases from 100 m to 400 m (the variation of H_{ch} changes from −50% to 100% of its original value in Fig. 5). This result was also demonstrated by Gannon and von Backström (2000) and Ming et al. (2006).

With the increase of the chimney diameter D_{ch} from 15 m to 60 m (the variation of D_{ch} changes from −50% to 100% of its original value in Fig. 5), its effect on the generation efficiency is a parabolic trend, which increases from 0.12% to the maximum 0.18% and later reduces to 0.17%. On the one hand, the increase of D_{ch} improves the air mass flow rate, on the other hand it reduces the area of the solar collector and decreases the air heating. Due to the combined effects of the two factors, the power output firstly increases and then decreases. Thus, there exists the optimal chimney diameter for the maximum generation efficiency.

When the solar collector radius R_{col} increases from 100 m to 400 m (the variation of R_{col} changes from −50% to 100% of its original value in Fig. 5), the generation efficiency decreases slowly. It is because that the total solar energy collected by the collector enhances with the increase of R_{col} and the density of the indoor air reduces when it absorbs more irradiation, which results in the improvement of the power output. However, when the air temperature is high, the heat loss from the collector to the environment also increases. In this case, the percentage increase of the power output is less than that of the input solar energy because of the increase of energy loss. Thus, the generation efficiency which is the ratio of the power output to the total input solar energy will decrease slightly. The same result is also indicated in the study of Haaf et al. (1983).

The solar collector height H_{col} has slight effect on the generation efficiency of SCPPs, which slowly increases at first and then slowly decreases with the increase of H_{col}. When H_{col} is small, $\frac{C_5^t}{R_{col}H_{col}^3} \gg \frac{C_6^t H_{ch}}{D_{ch}^5}$, the air mass flow is primarily influenced by H_{col}. The increase of H_{col} leads the increase of the air mass flow rate, thus the power output increases. But when H_{col} increases to a certain value, $\frac{C_5^t}{R_{col}H_{col}^3} \ll \frac{C_6^t H_{ch}}{D_{ch}^5}$, the air mass flow is then mainly controlled by the chimney diameter. However, the velocity of the air mass flow decreases with the increase of H_{col}, which results in the reduction of the heat exchange between the air and the heat storage layer. Thus, the air temperature rise decreases and the air density increases, thereby the power output and the generation efficiency reduce.

Since the heat storage layer is used to store solar energy, it only affects the distribution of the power generation in the day and the night. The thickness of the heat storage layer has little influence on the generation efficiency of SCPPs.

4.2.2. The influence of geometric parameters on the power stability

Fig. 6 shows the influences of geometric parameters on the power stability of SCPPs. It can be seen that the chimney height, the chimney diameter, the solar collector radius, the solar collector height, and the heat storage layer thickness, all have obviously influences on the power stability.

The chimney diameter D_{ch} is one of the most important factors which impacts on the power stability. There is a negative correlation between D_{ch} and the generation efficiency. The system power stability reduces from 0.897 to 0.855 with the increase of D_{ch} from 10 m to 60 m (the variation of D_{ch} changes from −50% to 100% of its original value in Fig. 6). It can be seen from Eq. (23) that the increase of D_{ch} causes the increase of air mass flow, which results in the velocity increase of the air flow and the improvement of the convective heat transfer between the air and the heat storage layer. Therefore, the solar energy absorbed by the air increases and the thermal energy stored in the heat storage layer decreases during the daytime. While at the nighttime, the surface temperature of the heat storage layer is low because the thermal energy released from the heat storage layer decreases. In this case, the air temperature difference between the daytime and the nighttime is large, which leads poor system power stability.

The power stability decreases slightly when the chimney height H_{ch} increases. According to Eq. (23), the air mass flow rate increases slightly with the increase of H_{ch}, which improve the convective heat transfer between the air and the heat storage layer. Similar to the above analysis of the change of D_{ch}, the system power stability decreases.

The solar collector radius R_{col} has a positive correlation with the system power stability. When R_{col} increases from 100 m to 400 m (the variation of R_{col} changes from −50% to 100% of its original value in Fig. 6), the power stability increases from 0.861 to 0.883. The air temperature increases and its density decreases as the area of the solar collector increases, which leads to the reduction of the convective heat transfer coefficient between the air and the heat storage layer surface. Therefore, during day, there is more thermal energy stored in the heat storage layer which can be released at night. Then, the air temperature difference between the daytime and nighttime reduces, which improves the system power stability.

The system power stability rises significantly when the solar collector height H_{col} increases from 0.75 m to 3 m (the variation of solar collector height changes from −50% to 100% of its original value in Fig. 6). The air flow velocity decreases with the increase of H_{col}, which results in the reduction of the convective heat transfer coefficient between the air and the heat storage layer surface. Therefore, the air temperature difference between the day and the night reduces and the system power stability is enhanced.

With the increase of the thickness of the heat storage layer δ_s, the trend of its influence on the power stability is parabolic. The power stability reaches the maximum 0.867 when δ_s is about 2.00 m. The thermal energy storage capacity firstly increases with the increase of δ_s and more solar energy can be accumulated in the heat storage layer during day and be released at night, which improves the power stability. However, when δ_s increases to a certain value, the thicker δ_s prevents the release of the thermal energy at night due to the relatively small conductivity of soil, which reduces the power stability.

4.3. Geometric parameters optimization

The power quality factor proposed in Section 3 is employed to optimize geometric parameters of SCPPs to obtain the better power generation performance. Fig. 7 shows the influences of different geometric parameters on the power quality factor.

The optimization results indicate that there is a strong positive correlation between H_{ch} and the power quality factor. According to the analysis in Sections 4.2.1 and 4.2.2, the system generation efficiency increases with the increase of H_{ch}, while H_{ch} has little negative influence on the power stability. But overall, the power generation quality of SCPPs improves with the increase of H_{ch}.

The power quality factor has a negative correlation with R_{col}. It is because that, with the increase of R_{col}, the generation efficiency decreases while the power stability improves. However, R_{col} has a greater influence on the efficiency than that on the power stability. Therefore, the system power quality factor decreases with the increase of R_{col}. Moreover, power quality factors are parabolic trends with the increases of the chimney diameter D_{ch}, the solar collector height H_{col} and the heat storage layer thickness δ_s, as shown in Fig. 7. Thus, there exists optimal values of D_{ch}, H_{col}, and δ_s. A SCPP system with 200 m-high chimney, 180 m-radius solar collector, and other parameters as same as those in Spain Manzanares demonstration power plant is taken as the case study. The coupling influences of D_{ch}, H_{col} and δ_s on the power quality factor are shown in Fig. 8. It can be seen that D_{ch} is one of the important factors that impacts the power generation quality. The increase of D_{ch} significantly enhances the power quality factor. Moreover, it is obviously that there is a strong coupling relation between D_{ch} and H_{col}. The relationship between the power quality factor and H_{col} with the same D_{ch} is parabola curve. Besides, the optimal H_{col} increases with the increase of D_{ch}. For instance, the optimal H_{col} increases from 0.3 m to 2.0 m when D_{ch} increases from 10 m to 30 m. This is because the air mass flow rate is both affected by the chimney diameter and the solar collector height.

The approximate expression of the relationship between the optimal solar collector height and the chimney diameter is shown in Eq. (28) based on the simulation results of the SUMM.

$$H_{col,opt} = 0.0024D_{ch}^2 - 0.0128D_{ch} + 0.22 \quad (28)$$

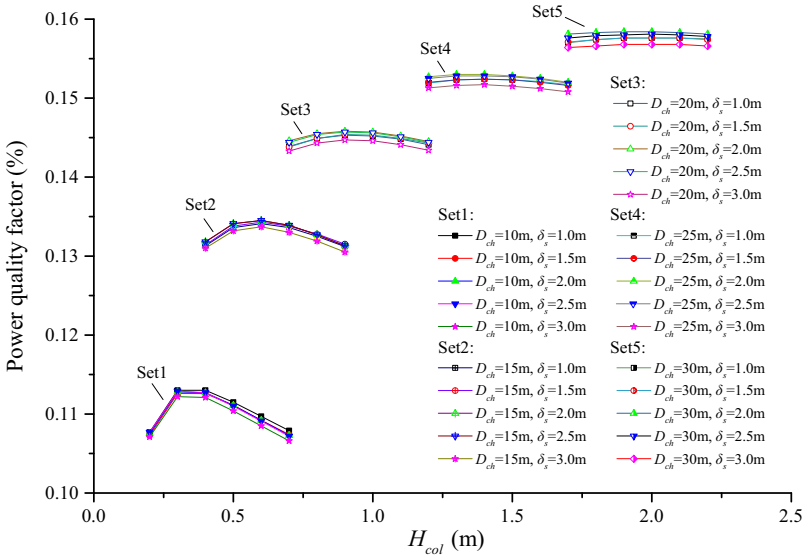

Fig. 8. Coupling influences of geometric parameters on power quality factor.

Eq. (28) indicates that optimal solar collector height and the chimney diameter presents a quadratic function relation. Therefore, the optimal solar collector height is 1.40 m when the chimney diameter is 25 m, or, the optimal solar collector height is 2.00 m when the chimney diameter is 30 m.

For a SCPP system, the heat storage layer is related with the system power stability, and the optimal thickness of the heat storage layer mainly depends on thermal physical parameters (such as the heat capacity and the thermal conductivity) of the heat storage material. Due to the cheap cost, soil is usually used as the material for heat storage layer. As showed in Fig. 8, the chimney diameter and the solar collector height impact little on the optimal thickness of the soil heat storage layer. The optimal thickness of the heat storage layer of soil in this case is about 2.00 m.

5. Conclusions

In this paper, the UCMM is proposed to analysis the energy conversion and transmission of SCPPs. In order to overcome the complexity of the UCMM, the SUMM is derived to simplify the analysis of the influence of the system geometric parameters on the power output of SCPPs. The simulation results show that both of the UCMM and the SUMM have sufficiently accuracy with experimental results. In addition, given the generation efficiency of SCPPs and the safety of the power grid, the power quality factor is put forward to comprehensively evaluate the power generation quality of SCPPs from the view of quantity and quality.

The research results indicate that the generation efficiency of SCPPs is mainly affected by the chimney height. And the chimney diameter, the solar collector radius, the collector height, and the heat storage layer thickness, impact on the generation efficiency in a limited way. There is a positive correlation between the chimney height and the generation efficiency, as well as the solar collector radius has a negative correlation with the generation efficiency. Moreover, there exist the optimal chimney diameter and the optimal collector height to maximize the generation efficiency. The power stability of SCPPs is also influenced by geometric parameters. The increases of the radius and the height of the solar collector, and the decreases of the height and the diameter of the chimney, as well as the appropriate storage layer thickness, can improve the power stability of SCPPs.

The geometric optimization results show that there are a strong positive correlation between the chimney height and the power quality factor, as well as a negative correlation between the solar collector radius and the power quality factor. Moreover, the solar collector height has a coupling relationship with the chimney diameter. There are optical values of the chimney diameter and the solar collector height to achieve the best power generation quality of SCPPs. The optimal thickness of the soil heat storage layer is little affected by other geometric parameters. For a SCPP with 200 m-high chimney, 180 m-radius solar collector and soil heat storage layer, the optimal solar collector height is a quadratic function relation with the chimney diameter, and the optimal thickness of the heat storage layer is 2.00 m. Further works should take the investment into account the indicator to comprehensively optimize the structure design of SCPPs.

Conflicts of interest

The authors declare that there are no conflicts of interest.

Acknowledgment

This project is supported by the National Basic Research Program of China (Grant No. 2015CB251505) and the Fundamental Research Funds for the Central Universities (No. 2016YXZD009, HUST).

References

Alawin, A., Badran, O., Awad, A., Abdelhadi, Y., Al-Mofleh, A., 2013. Feasibility study of a solar chimney power plant in Jordan. Appl. Sol. Energy 48, 260–265.
Asnaghi, A., Ladjevardi, S.M., 2012. Solar chimney power plant performance in Iran. Renew. Sustain. Energy Rev. 16, 3383–3390.
Bernardes, M.A.d.S., Voß, A., Weinrebe, G., 2003. Thermal and technical analyses of solar chimneys. Sol. Energy 75, 511–524.
Bernardes, M.A.d.S., 2010. Solar chimney power plants developments and advancements. Sol. Energy, 171–186.
Bernardes, M.A.d.S., Zhou, X.P., 2013. On the heat storage in Solar Updraft Tower collectors-water bags. Sol. Energy 91, 22–31.
Gannon, A.J., von Backström, T.W., 2000. Solar chimney cycle analysis with system loss and solar collector performance. J. Sol. Energy Eng. 122, 133–137.
Cottam, P.J., Duffour, P., Lindstrand, P., Fromme, P., 2016. Effect of canopy profile on solar thermal chimney performance. Sol. Energy 129, 286–296.
Dehghani, S., Mohammadi, A.H., 2014. Optimum dimension of geometric parameters of solar chimney power plants – a multi-objective optimization approach. Sol. Energy 105, 603–612.

Gholamalizadeh, E., Kim, M.H., 2014. Thermo-economic triple-objective optimization of a solar chimney power plant using genetic algorithms. Energy 70, 204–211.
Guo, P.H., Li, J.Y., Wang, Y., Liu, Y.W., 2013. Numerical analysis of the optimal turbine pressure drop ratio in a solar chimney power plant. Sol. Energy 98, 42–48.
Guo, P.H., Li, J.Y., Wang, Y., Liu, Y.W., 2015. Numerical study on the performance of a solar chimney power plant. Energy Convers. Manage. 105, 197–205.
Haaf, W., Friedrich, K., Mayr, G., et al., 1983. Solar chimneys, Part I: principle and construction of the pilot plant in Manzanares. Int. J. Solar Energy 2, 3–20.
Haaf, W., 1984. Solar chimneys, part II: preliminary test results from the Manzanares pilot plant. Int. J. Sol. Energy 2, 141–161.
Hamdan, M.O., 2013. Analysis of solar chimney power plant utilizing chimney discrete model. Renew. Energy 56, 50–54.
Li, W.B., Wei, P., Zhou, X.P., 2014. A cost-benefit analysis of power generation from commercial reinforced concrete solar chimney power plant. Energy Convers. Manage. 79, 104–113.
Liu, J.M., 2010. Solar Energy Utilization: Principle, Technology and Engineering. Electronic Industry Press, Beijing, China.
Kasaeian, A., Ghalamchi, M., Ghalamchi, M., 2014. Simulation and optimization of geometric parameters of a solar chimney in Tehran. Energy Convers. Manage. 83, 28–34.
Koonsrisuk, A., Lorente, S., Bejan, A., 2010. Constructal solar chimney configuration. Int. J. Heat Mass Transf. 53, 327–333.
Koonsrisuk, A., Chitsomboon, T., 2013. Effects of flow area changes on the potential of solar chimney power plants. Energy 51, 400–406.
Kreetz, H., 1997. Theoretische untersuchungen und auslegung eines tempor. Diplomarbeit TU Berlin, Berlin.
Maia, C.B., Ferreira, A.G., Valle, R.M., Cortez, M.F.B., 2009. Theoretical evaluation of the influence of geometric parameters and materials on the behavior of the airflow in a solar chimney. Comput. Fluids 38, 625–636.
Ming, T.Z., Liu, W., Xu, G.L., 2006. Analytical and numerical investigation of the solar chimney power plant systems. Int. J. Energy Res. 30, 861–873.
Ming, T.Z., Wang, X.J., de Richter, R.K., Liu, W., Wu, T.H., Pan, Y., 2012. Numerical analysis on the influence of ambient crosswind on the performance of solar updraft power plant system. Renew. Sustain. Energy Rev. 16, 5567–5583.
Ming, T.Z., Meng, F.L., Liu, W., Pan, Y., de Richter, R.K., 2013. Analysis of output power smoothing method of the solar chimney power generating system. Int. J. Energy Res. 37, 1657–1668.
Mullett, L.B., 1987. The solar chimney-overall efficiency, design and performance. Int. J. Ambient Energy 8, 35–40.
Nizetic, S., Klarin, B., 2010. A simplified analytical approach for evaluation of the optimal ratio of pressure drop across the turbine in solar chimney power plants. Appl. Energy 87, 587–591.
Pasumarthi, N., Sherif, S.A., 1998a. Experimental and theoretical performance of a demonstration solar chimney model-Part I: mathematical model development. Int. J. Energy Res. 22, 277–288.
Pasumarthi, N., Sherif, S.A., 1998b. Experimental and theoretical performance of a demonstration solar chimney model-Part II: experimental and theoretical results and economic analysis. Int. J. Energy Res. 22, 443–461.
Papageorgiou, C.D., 2013. Enclosed Solar Chimney Technology <http://www.gchimneytech.com/technology.html>.
Patel, S.K., Prasad, D., Ahmed, M.R., 2014. Computational studies on the effect of geometric parameters on the performance of a solar chimney power plant. Energy Convers. Manage. 77, 424–431.
Pretorius, J.P., Kröger, D.G., 2006a. Critical evaluation of solar chimney power plant performance. Sol. Energy 80, 535–544.
Pretorius, J.P., Kröger, D.G., 2006b. Solar chimney power plant performance. J. Sol. Energy Eng. 128, 302–311.
Pretorius, J.P., Kröger, D.G., 2007. Sensitivity analysis of the operating and technical specifications of a solar chimney power plant. J. Solar Energy Eng. 129, 171–178.
Pretorius, J.P., Kröger, D.G., 2008. Thermoeconomic optimization of a solar chimney power plant. J. Sol. Energy Eng. 130 (021015), 1–9.
Pretorius, J.P., Kröger, D.G., 2009. The influence of environment on solar chimney power plant performance. Res. Develop. J. South Afr. Inst. Mech. Eng. 25, 1–9.
Schlaich, J., 1995. The Solar Chimney: Electricity from the Sun. Edition Axel, Menges, Stuttgart, Germany.
Schlaich, J., Bergermann, R., Schiel, W., Weinrebe, G., 2005. Design of commercial solar updraft tower systems-utilization of solar induced convective flows for power generation. J. Sol. Energy Eng. 127, 117–124.
Shariatzadeh, O.J., Refahi, A.H., Abolhassani, S.S., Rahmani, M., 2015. Modeling and optimization of a novel solar chimney cogeneration power plant combined with solid oxide electrolysis/fuel cell. Energy Convers. Manage. 105, 423–432.
Tu, C.J., Shen, L.C., Wu, Z.J., 1992. Heat Conduction. Higher Education Press, Beijing, China.
Xu, Y.Y., Zhou, X.P., Cheng, Q., 2015. Performance of a large-scale solar updraft power plant in a moist climate. Int. J. Heat Mass Transf. 91, 619–629.
Zhou, X.P., Yang, J.K., Xiao, B., Hou, G.X., 2007. Simulation of a pilot solar chimney power equipment. Renew. Energy 32, 1637–1644.
Zhou, X.P., Yang, J.K., Xiao, B., Hou, G.X., Xing, F., 2009. Analysis of chimney height for solar chimney power plant. Appl. Therm. Eng. 29, 178–185.
Zhou, X.P., Xu, Y.Y., 2016. Solar updraft tower power generation. Sol. Energy 128, 95–125.
Zou, Z., Guan, Z.Q., Gurgenci, H., 2013. Optimization design of solar enhanced natural draft dry cooling tower. Energy Convers. Manage. 76, 945–955.